M.F. Insana and R.M. Leahy (Eds.): IPMI 2001,
Lecture Notes in Computer Science **2082**:259-271, 2001

Estimability of Spatio-temporal Activation In fMRI

Andre Lehovich[1,2,3], Harrison H. Barrett[1,2,3,4],
Eric W. Clarkson[1,2,3,4] and Arthur F. Gmitro[2,4]

[1] Center for Gamma-Ray Imaging, University of Arizona, Tucson AZ 85721, USA
http://gamma.radiology.arizona.edu Lehovich@math.arizona.edu
[2] Department of Radiology, University of Arizona
[3] Program in Applied Mathematics, University of Arizona
[4] Optical Sciences Center, University of Arizona

Abstract. Event-related functional magnetic resonance imaging (fMRI) is considered as an estimation and reconstruction problem. A linear model of the fMRI system based on the Fourier sampler (k-space) approximation is introduced and used to examine what parameters of the activation are estimable, i.e. can be accurately reconstructed in the noise-free limit. Several possible spatio-temporal representations of the activation are decomposed into null and measurement components. A causal representation of the activation using generalized Laguerre polynomials is introduced.

1 Introduction

In functional magnetic resonance imaging (fMRI), the signal is produced by a temporary physiologically induced change in the magnetization of a brain region. This change is called the activation. (For an introduction to fMRI see [15].) Most prior work has considered fMRI to be a *signal-detection* problem: for a given region of interest in the brain, usually a voxel, did the average magnetization significantly change after the subject received some stimulus? Typically the results of signal detection on many voxels are displayed as an activation map. Instead, we focus on fMRI as an *estimation* problem: how much has the average magnetization in the region changed t seconds after the stimulus?

We prefer estimation to signal detection for several reasons: First, there has been much debate over the optimal signal-detection strategy. Yet we know from other signal-detection problems that good understanding of the signal is helpful in formulating the optimal detection strategy. Second, in many signal-detection algorithms the first step is to estimate the signal. Third, detection reduces the data to a binary value (or activation map of binary values), yet information about the signal magnitude might be of interest. Finally, without knowledge about the true activation it is difficult to produce the ROC curves needed to compare the performance of different signal-detection systems.

In any imaging system the accuracy of estimates (reconstructions) is affected by factors such as measurement noise, errors in the mathematical model of the

imaging system, and those aspects of an object that the system is incapable of measuring. The latter is the focus of this paper. We answer the question "In the best case of noise-free data and no modeling error, what parameters of the activation can we linearly estimate using data from an fMRI system?" (We consider the fMRI system to include both the MRI hardware and the scan sequence software.) An equivalent but perhaps more interesting question is "Even with the generous assumptions of no noise and no modeling error, what parameters of the activation can we not reconstruct?" Answering these questions allows us to compare the tradeoffs in spatial vs. temporal resolution of different scan sequences.

In section 2 we present a linear model relating the fMRI measurements to the activation we wish to reconstruct and the parameters that must be estimated. Our model explicitly treats the activation as a spatio-temporal function and the imaging system as a continuous-to-discrete[1] mapping. Several ways to represent the activation are suggested, including a novel representation using generalized Laguerre polynomials. In section 3 we introduce estimability and the decomposition of activation viewed through an fMRI system into null and measurement components. This decomposition tells us for a specific fMRI system what can be accurately reconstructed in the absence of measurement noise. The same analysis can be used either to match the activation representation to a specific imaging system or to optimize the fMRI system for a given activation representation. In section 4 we compute the measurement and null components of several representations of the activation.

2 Linear Model & The fMRI Inverse Problem

Our model of the imaging process begins with the spatial Fourier sampler (k-space) approximation derived in most texts, including [13] and [12]. The basic measurement equation is

$$g_j \triangleq \int\!\!\int M(\boldsymbol{r},t) e^{-2\pi i \boldsymbol{r}\cdot\boldsymbol{k}(t)} p(t-t_j)\, d\boldsymbol{r}\, dt + n_j, \tag{1}$$

where $\boldsymbol{g}$ is measured, $M(\boldsymbol{r},t)$ is the transverse magnetization in the rotating frame at time t, the spatial Fourier components $\boldsymbol{k}(t)$ are controlled by the scan sequence software, $p(t-t_j)$ is the temporal sampling blur of the MRI hardware, and $\boldsymbol{n}$ is zero-mean white Gaussian noise. (Field strength, excitation/echo times, and other details of the MRI system are included in $M(\boldsymbol{r},t)$, as are facets of the experimental subject such as $T_2^*(\boldsymbol{r},t)$.)

Mental activity causes a temporary change in $M(\boldsymbol{r},t)$. The magnetization can be partitioned into baseline equilibrium and activation components

$$M(\boldsymbol{r},t) \triangleq M^{\mathrm{eq}}(\boldsymbol{r},t) + \delta M(\boldsymbol{r},t). \tag{2}$$

[1] The activation function is defined on a continuous set of points, but need not be a continuous function in the usual sense; for example, discontinuities might occur at anatomical boundaries.

Combining (1) and (2) gives

$$\boldsymbol{g} \stackrel{\triangle}{=} \boldsymbol{g}^{\mathrm{eq}} + \boldsymbol{\Delta g} \tag{3}$$

$$g_j = \iint M^{\mathrm{eq}}(\boldsymbol{r},t) e^{-2\pi i \boldsymbol{r}\cdot\boldsymbol{k}(t)} p(t-t_j)\, d\boldsymbol{r}\, dt + \iint \delta M(\boldsymbol{r},t) e^{-2\pi i \boldsymbol{r}\cdot\boldsymbol{k}(t)} p(t-t_j)\, d\boldsymbol{r}\, dt + n_j. \tag{4}$$

In an fMRI experiment using the event-related paradigm the subject is asked to perform a cognitive task[2] after being exposed to a stimulus [10]. For example, the subject might be shown a stimulus of three letters with the task to think of a word beginning with that syllable. During the experiment the MRI system records data by repeatedly executing a scan sequence. Because the change in magnetization produces a change in data of similar magnitude to the noise, the stimulus cycle is often repeated many times to average over noise realizations. In the discussion below we will use index c to denote the stimulus cycle, index s to denote the scan sequence repetition within the cycle, and index j to denote a measurement within the scan sequence.

We assume that the activation is reproducible over stimulus cycles[3] and that the magnetization is linear with the number of stimuli, so

$$\delta M(\boldsymbol{r},t) = \sum_{t_l<t} f(\boldsymbol{r}, t-t_l), \tag{5}$$

where $f(\boldsymbol{r},t)$ is the activation due to only one stimulus, and t_l is the time of stimulus number l. We assume that the activation is spatially $\mathbb{L}_2$ and therefore has an infinite-series representation

$$\int |f(\boldsymbol{r},t)|^2\, d\boldsymbol{r} < \infty,\ \forall t \Rightarrow f(\boldsymbol{r},t) = \sum_{m=1}^{\infty} \alpha_m(t)\phi_m(\boldsymbol{r}). \tag{6}$$

We also assume that the activation decays quickly enough to be temporally $\mathbb{L}_2$, so $\alpha_m(t)$ also has an infinite series representation

$$\int_0^{\infty} |f(\boldsymbol{r},t)|^2\, dt < \infty,\ \forall \boldsymbol{r} \Rightarrow \alpha_m(t) = \sum_{n=1}^{\infty} \alpha_{mn}\psi_n(t). \tag{7}$$

Therefore the activation can be exactly represented as an infinite series

$$f(\boldsymbol{r},t) = \sum_{m=1}^{\infty}\sum_{n=1}^{\infty} \alpha_{mn}\phi_m(\boldsymbol{r})\psi_n(t). \tag{8}$$

[2] The experimental subject's cognitive task should not be confused with the imaging task, which is either signal detection or parameter estimation.

[3] This popular assumption is probably not true. We make it in keeping with the best-possible-case spirit of our analysis.

Substituting (5) and (8) into (4) and assuming the same scan sequence is always used gives the final signal equation:

$$\begin{aligned} g_{csj} &= g_{sj}^{\mathrm{eq}} + \Delta g_{csj} \\ &= \iint M^{\mathrm{eq}}(\boldsymbol{r}, t) e^{-2\pi i \boldsymbol{r}\cdot\boldsymbol{k}(t)} p(t - t_{csj})\, d\boldsymbol{r}\, dt \\ &\quad + \iint e^{-2\pi i \boldsymbol{r}\cdot\boldsymbol{k}(t)} p(t - t_{csj}) \sum_{l=1}^{c} \sum_{m=1}^{\infty} \sum_{n=1}^{\infty} \alpha_{mn} \phi_m(\boldsymbol{r}) \psi_n(t - t_l)\, d\boldsymbol{r}\, dt \\ &\quad + n_{csj}. \end{aligned} \tag{9}$$

The inverse problem in fMRI is to find the activation $f(\boldsymbol{r}, t)$ by estimating α_{mn} for a convenient representation $\phi_m(\boldsymbol{r})\psi_n(t)$ from data g_{csj}. In practice the sums in (9) must be truncated to a finite number of terms.

2.1 Various Activation Representations

There are many possible ways to represent the activation. Motivated by (8), in this paper we consider only representations where each element can be written as the product of a spatial function $\phi_m(\boldsymbol{r})$ and a temporal function $\psi_n(t)$.

Spatial Representations Voxels are the most popular choice of spatial elements. Advantages of voxels include a simple physical interpretation and tiling with no overlap of elements. However, voxels do not correspond to any meaningful anatomical features, and voxel boundaries do not conveniently line up with the boundaries of different brain regions. The voxel's long tails in the Fourier domain pose an additional problem.

Kaiser-Bessel blobs provide another possible spatial representation. (For the definition and many nice properties of Kaiser-Bessel blobs see [11].) Unlike voxels, blobs do not tile space; but they do have compact support in either the space or frequency domain and almost compact support in the other.

A third choice is anatomical "pixels", which provide an easy way of building prior information into the reconstruction. A neurophysiologist would trace out regions in which the average activation is of interest on a high-resolution scout scan of the subject. These regions might be small (part of a gyrus), or might be large (the hippocampus). Because α_{ij} are estimated directly from k-space data, the analyst could compare competing models of neuroanatomy by reconstructing onto several representations. (A representation with one anatomical pixel is considered in [14].)

Temporal Representations Three choices of temporal representation are of interest. Point samples $\delta(t - t_i)$ are popular, but don't tell us anything about what is happening between samples. Sinc functions,

$$\mathrm{sinc}(t - t_i) = \frac{\sin\left[\pi(t - t_i)\right]}{\pi(t - t_i)}, \tag{10}$$

provide smooth interpolation and are useful if the activation has temporal bandcutoff B and the sample rate is fast enough that $\delta t_s < 1/(2B)$. However, the tail on sinc extends to time $t = -\infty$, violating causality.

Functions of the form $Ct^n e^{-\beta t}$, with n, β free parameters and C a normalizing constant are called gamma functions in the fMRI literature and have been used to model the activation [5]. A gamma function is similar to the expected activation profile at lower field strengths: starting at zero, increasing to a peak, and then decaying back to zero. Disadvantages of a gamma function representation include inability to represent an activation profile with the initial negative dip expected to be observable at higher field strengths [8], and the nonlinear regression required to fit n and β.

Both problems are overcome by a causal representation using generalized Laguerre polynomials weighted by $\sqrt{t^3 e^{-t}}$. These functions are orthonormal in the interval $[0, \infty)$. (For many nice properties of generalized Laguerre polynomials see [1]. The first three are shown in figure 1.) Because the generalized Laguerre polynomials are a basis for temporal $\mathbb{L}_2$, any activation profile can be represented by enough terms. Since the envelope is similar to the anticipated activation, the activation can be represented using only a few elements, leading to a dimensionality reduction from the number of samples in one stimulus cycle. The sinc representation has as many elements as time points at which f is sampled, requiring many stimulus cycles to average over noise. The causal representation uses fewer elements and therefore has better noise averaging, allowing fewer stimulus cycles.

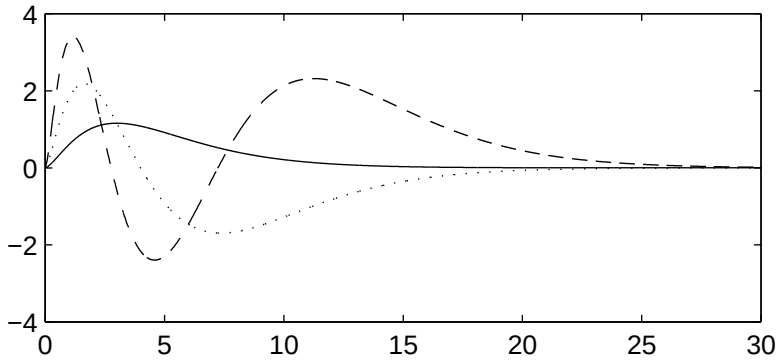

Fig. 1. The 3rd order generalized Laguerre orthonormal polynomials weighted with $\sqrt{t^3 e^{-t}}$ form a causal basis in time. The first three functions are displayed. $\psi_1(t) = \sqrt{t^3 e^{-t}}$ (*solid*), $\psi_2(t) = (4-t)\psi_1(t)$ (*dotted*), $\psi_3(t) = (10 - 5 * t + t^2/2)\psi_1(t)$ (*dashed*).

3 Null Space and Estimability

The signal equation (9) can be rewritten

$$\Delta \boldsymbol{g} = \mathcal{H} f(\boldsymbol{r}, t) + \boldsymbol{n} \tag{11}$$

$$\Delta g_{csj} = \iint h_{csj}(\boldsymbol{r}, t) f(\boldsymbol{r}, t)\, d\boldsymbol{r}\, dt + n_{csj} \tag{12}$$

$$h_{csj}(\boldsymbol{r}, t) = e^{-2\pi i \boldsymbol{r}\cdot\boldsymbol{k}(t)} \sum_{l=1}^{c} p(t - t_{csj} + t_l) \tag{13}$$

where $\mathcal{H}$ is a continuous-to-discrete linear operator with kernel $h_{csj}(\boldsymbol{r}, t)$. Because $\mathcal{H}$ maps an infinite Hilbert space to a finite-dimensional space, it is not invertible and must have a non-trivial null-space. The null space consists of the functions the fMRI system maps to zero, a generalization of the concept of system blind spots. Any spatio-temporal function $q(\boldsymbol{r}, t)$ can be decomposed into orthogonal null and measurement components

$$q(\boldsymbol{r}, t) = q_{\text{meas}}(\boldsymbol{r}, t) + q_{\text{null}}(\boldsymbol{r}, t), \tag{14}$$

where $\mathcal{H} q_{\text{null}}(\boldsymbol{r}, t) = 0$ and $\mathcal{H} q(\boldsymbol{r}, t) = \mathcal{H} q_{\text{meas}}(\boldsymbol{r}, t)$. (See chapter 7 in [3] for further discussion on this decomposition.) Because no information about $q_{\text{null}}(\boldsymbol{r}, t)$ passes through the fMRI system, without strong prior information about $q(\boldsymbol{r}, t)$ it is impossible to accurately reconstruct $q_{\text{null}}(\boldsymbol{r}, t)$, hence $q(\boldsymbol{r}, t)$, from the data even in the absence of measurement noise.

The projection operators $\mathcal{M}$ and $\mathcal{N}$ onto the measurement and null spaces respectively are defined

$$\mathcal{M} q(\boldsymbol{r}, t) = \mathcal{H}^{+} \mathcal{H} q(\boldsymbol{r}, t) \tag{15}$$

$$\mathcal{N} q(\boldsymbol{r}, t) = q(\boldsymbol{r}, t) - \mathcal{M} q(\boldsymbol{r}, t), \tag{16}$$

where $\mathcal{H}^{+}$ is the Moore-Penrose pseudoinverse. (See chapters 9-10 of [4] for an introduction to uses of the pseudoinverse in imaging. The Moore-Penrose pseudoinverse for a Fourier sampler is derived in [16].) The null component of a function is zero if and only if the function can be written as a linear combination of the kernels:

$$\mathcal{N}\{q(\boldsymbol{r}, t)\} = 0 \Leftrightarrow q(\boldsymbol{r}, t) = \sum_{csj} b_{csj} h_{csj}(\boldsymbol{r}, t). \tag{17}$$

3.1 Estimable Parameters of the Activation

A linear parameter (functional) of the activation

$$\theta(f(\boldsymbol{r}, t)) = \iint f(\boldsymbol{r}, t) T(\boldsymbol{r}, t)\, d\boldsymbol{r}\, dt \tag{18}$$

is said to be *estimable* from the data if there exists a vector $\boldsymbol{w}$ such that

$$\theta(f(\boldsymbol{r}, t)) = \left\langle \boldsymbol{w}^{\dagger} \boldsymbol{g} \right\rangle_n = \boldsymbol{w}^{\dagger} (\mathcal{H} f(\boldsymbol{r}, t) + \langle \boldsymbol{n} \rangle) = \boldsymbol{w}^{\dagger} \mathcal{H} f(\boldsymbol{r}, t) \tag{19}$$

where † means adjoint (transpose and complex conjugate) and $\langle\cdot\rangle$ is expected value [2]. (If θ is estimable then $\boldsymbol{w}^\dagger \boldsymbol{g}$ is an unbiased estimator.) Estimable parameters can be accurately reconstructed in the noise-free limit. By partitioning into orthogonal null and measurement components, (18) becomes

$$\begin{aligned}\theta(f(\boldsymbol{r},t)) = &\iint f_{\text{meas}}(\boldsymbol{r},t) T_{\text{meas}}(\boldsymbol{r},t)\, d\boldsymbol{r}\, dt \\ &+ \iint f_{\text{null}}(\boldsymbol{r},t) T_{\text{null}}(\boldsymbol{r},t)\, d\boldsymbol{r}\, dt. \end{aligned} \tag{20}$$

No cross terms are needed in (20) because null space is orthogonal to measurement space. Since no information about f_{null} passes through the fMRI system, θ is estimable only if the second integral in (20) is always 0, which would happen if either $f_{\text{null}}(\boldsymbol{r},t) = 0$ or $T_{\text{null}}(\boldsymbol{r},t) = 0$. The former would be the case only with strong prior knowledge about the activation. By (17) the latter is the case only if $T(\boldsymbol{r},t)$ is a sum of the measurement kernels $h_{csj}(\boldsymbol{r},t)$. Because the measurement kernels precisely describe which parameters of the object can be accurately reconstructed they are called "natural pixels" in [6].

To accurately solve the inverse problem in (9) it is desirable to choose an activation representation $\phi_m(\boldsymbol{r})\psi_n(t)$ such that α_{mn} is estimable using one's fMRI system. (Alternatively, one could fix the representation and change the fMRI system by choosing $\boldsymbol{k}(t)$ to minimize the second integral in (20). Heuristics for the special case of only one spatial element are given in [14].) In the case of orthogonal representation functions such as voxels and Laguerre polynomials we have $T(\boldsymbol{r},t) = \phi_m(\boldsymbol{r})\psi_n(t)$. For a non-orthogonal representation such as Kaiser-Bessel blobs, $T(\boldsymbol{r},t)$ is slightly more complicated; see the section on bi-orthogonal bases in chapter 4 of [3] for more details. Either way, the α_{mn} are not estimable for any of the representations $\phi_m(\boldsymbol{r})$ and $\psi_n(t)$ described above.

How useful is a non-estimable representation? To answer this we can proceed several different ways. First, we could make some minimal assumptions about the activation and rigorously bound $\|f_{\text{null}}(\boldsymbol{r},t)\|$, then use this bound to argue that the second integral in (20) is small [7]. We have been unable to derive any useful bounds, largely because we believe that $f(\boldsymbol{r},t)$ has an initial negative dip and our existing machinery works only for non-negative functions.

Second, we could assume a probability measure on $f(\boldsymbol{r},t)$ and use that to derive a distribution on $\iint f_{\text{null}}(\boldsymbol{r},t) T_{\text{null}}(\boldsymbol{r},t)\, d\boldsymbol{r}\, dt$. This is not currently feasible because of the difficulties in constructing a realistic measure on possible activations.

Third, we can compute $f_{\text{meas}}(\boldsymbol{r},t)$ for several "typical" activation profiles and $T_{\text{meas}}(\boldsymbol{r},t)$ for several reconstruction representations to see what information passes through the system [17]. Though not rigorous, this can be useful for determining what we can't reconstruct even before noise and modeling error make things more difficult. The results of several such calculations are given in the next section.

4 Computation Results

To examine the null and measurement components we first make the approximation that there is no temporal blur in the MRI hardware, so $p(t) = \delta(t)$ in (9). We also make the approximation that the activation is constant during the time interval of one scan sequence. First we compute the null and measurement decomposition of purely spatial objects, then purely temporal objects.

4.1 Spatial Null/Measurement Decomposition

In order to compute the null and measurement components of a spatial object we use the Moore-Penrose pseudoinverse for a Fourier sampler derived in [16]. Because $\mathcal{H}^+$ is a direct mapping from the irregularly sampled k-space data to a linear combination of plane waves no regridding or discrete Fourier transform (DFT) is used in the computation. For these decompositions we used a simulated scan sequence of 4096 samples along a spiral of Archimedes looping around the origin 24 times, $|\boldsymbol{k}_{\max}| = 1.0$, in one tomographic slice of k-space. This corresponds to a 24cm×24cm field of view with 0.5cm resolution and is similar to the sequences used in fMRI. The measurement and null components are complex-valued functions defined on a continuous domain which are then sampled to produce the displayed image.

Figure 2 shows the decomposition of a square voxel into null and measurement components. Because of the asymmetric sampling in k-space both $f_{\text{meas}}(\boldsymbol{r})$ and $f_{\text{null}}(\boldsymbol{r})$ are complex-valued functions defined $\forall \boldsymbol{r} \in \mathbb{R}^2$. The imaginary components are not displayed because they are almost two orders of magnitude smaller than the real components. Notice that the measurement component of the voxel is not uniform; activation in the center of the voxel is more heavily weighted than activation at the corners and activation outside the voxel also contributes to its measurement component. Because only a finite region of k-space is sampled both components have infinite support and extend outside the region shown. The usual MRI practice of displaying magnitude is misleading since both f_{null} and f_{meas} take on negative values. Figure 3 shows the same decomposition for a Kaiser-Bessel blob with radius .25cm.

Figure 4 shows the decomposition of one 3mm slice through a voxelized high resolution brain phantom into null and measurement components for the same simulated scan sequence. The phantom was created by scanning a brain with a T_2^* weighted sequence (1.5T GE Signa scanner with gradient echo, TE = 30ms, TR = 3000ms) and using conventional techniques to reconstruct onto a 1mm^2 grid. The Fourier transforms of each voxel were analytically computed and added together to produce the simulated k-space data, then $\mathcal{H}^+$ was applied to produce the measurement component. The imaginary portions are again almost two orders of magnitude smaller than the real portions, so we have not displayed them.

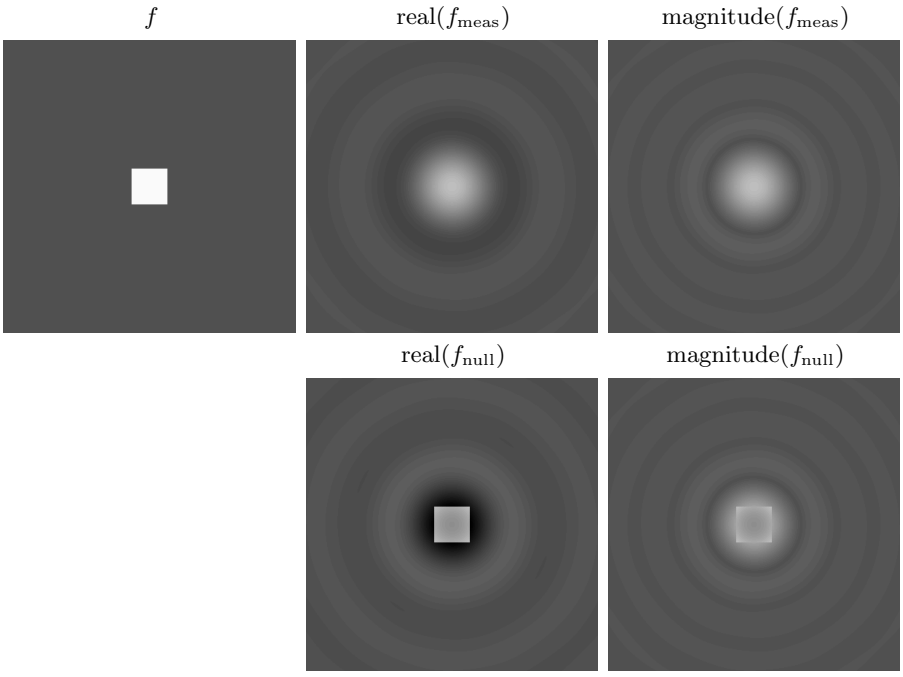

Fig. 2. Square .5cm^2 voxel partitioned into measurement-space and null-space components. Only the central 2cm×2cm of the 24cm×24cm are displayed. The linear grayscale ranges from -0.48 (black) to 1.0 (white). The gray shade in the background of f is 0. See text for description of the simulated scan sequence.

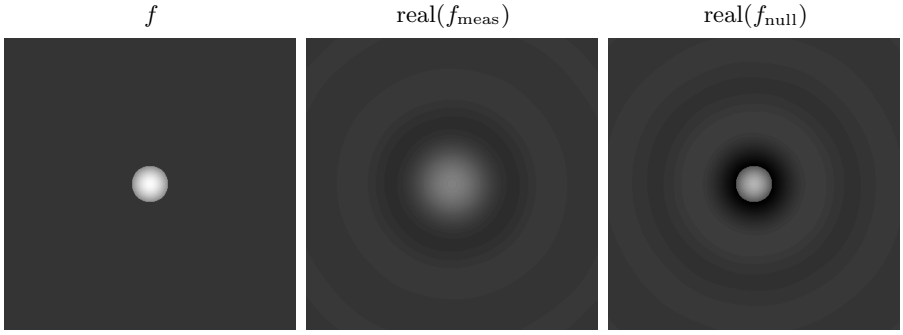

Fig. 3. Kaiser-Bessel blob of radius .25cm partitioned into measurement-space and null-space components. ($\alpha = 2.0$) The linear grayscale ranges from $-.28$ (black) to 1.0 (white).

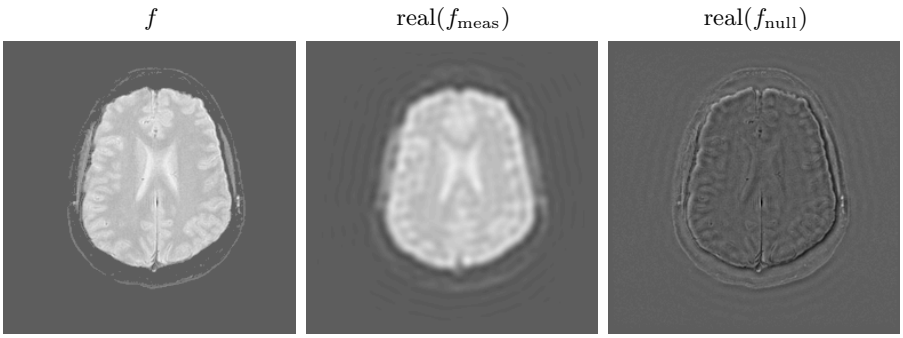

Fig. 4. Digital brain phantom partitioned into spatial measurement-space and null-space components. The linear grayscale ranges from −497 (black) to 850 (white).

4.2 Temporal Null/Measurement Decomposition

Figure 5 shows the decomposition of the first generalized Laguerre polynomial into null and measurement components. The function was point sampled every second, i.e. $h_l(t) = \delta(t - t_l)$. As always, the measurement component is the sum of the sensitivity functions and the null component is $f_{\text{null}} = f - f_{\text{meas}}$. Therefore the measurement component is the sum of weighted delta functions at the sampling times.

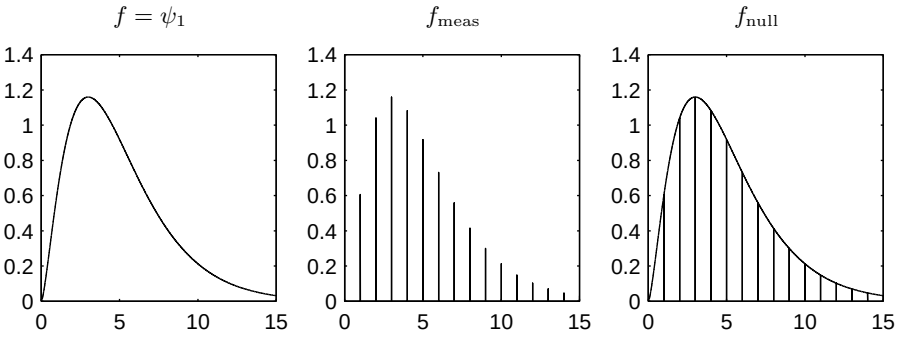

Fig. 5. First Laguerre polynomial $\psi_1(t) = \sqrt{t^3 e^{-t}}$ partitioned into measurement-space and null-space components for point sampling every second. The measurement component f_{meas} is the sum of weighted delta functions at the sample points and f_{null} is a smooth curve with holes at the sample points. Time is on the horizontal axis.

In practice delta functions are rarely used as a reconstruction representation. Instead some interpolation scheme is used to produce a smooth reconstruction. (One of the advantages of using a continuous activation representation is

that it provides a built-in interpolation scheme [9].) So instead of the measurement component, we should examine its reconstruction onto the representation $\sum_{n=1}^{n_{max}} \alpha_n \psi_n(t)$. If n_{max} is set to 6 and the α_n are chosen using the minimum norm least squares criterion then as expected $\alpha_1 = 1.0$ and the other coefficients are zero.

If a function can be written as the sum of a finite number of generalized Laguerre polynomials we refer to it as Laguerre-band-limited. (This is analogous to the more familiar Fourier-band-limited functions.) In practice we won't be lucky enough to have a Laguerre-band-limited function as the activation. In figure 6 we consider a triangle function sampled every second. For illustration purposes we have chosen to use only 6 generalized Laguerre polynomials in the reconstruction. Although not perfect, the reconstruction resembles the original and the reconstruction error is small. In figure 7 we reconstruct the same function sampled every three seconds. With the slower sampling time the reconstruction no longer resembles the original and the reconstruction error is large.

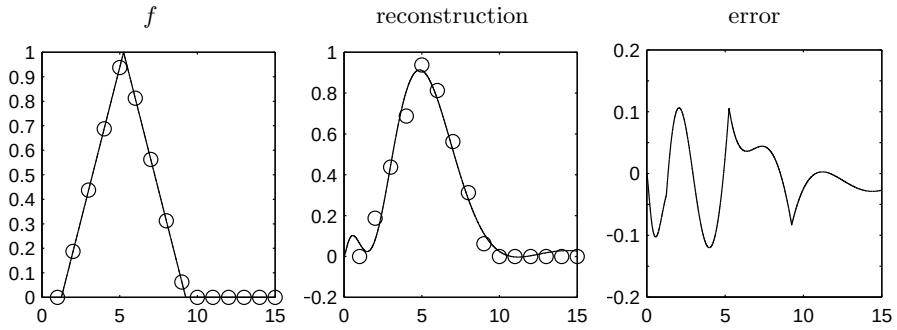

Fig. 6. Triangle function sampled every second and then reconstructed onto the first six generalized Laguerre polynomials. Circles indicate the times/values at which f was sampled. The error is the difference of f and the reconstruction. Time is on the horizontal axis.

5 Summary

In this paper we have presented a linear model for the fMRI measurement process and the inverse problem of reconstructing activation. Our model explicitly considers the fMRI system to be a continuous-to-discrete mapping. We suggested several candidate activation representations for solving the inverse problem, including a novel causal representation using generalized Laguerre polynomials. A causal representation may be useful in other spatio-temporal imaging problems such as first-pass cardiac imaging. We considered which parameters of the activation are estimable and examined the spatial and temporal null and measurement

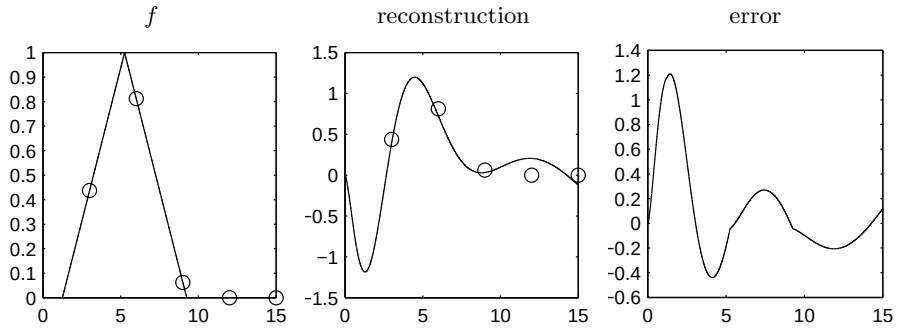

Fig. 7. Triangle function sampled every three seconds and then reconstructed onto the first six generalized Laguerre polynomials. Circles indicate the times/values at which f was sampled. The error is the difference of f and the reconstruction. Time is on the horizontal axis.

spaces of the fMRI system. The null/measurement decomposition can be used both to determine which activation representations can be reconstructed using a specific fMRI system and to tune the fMRI system so that a desired representation of the activation can be accurately reconstructed. In order to increase spatial resolution by sampling more k-space points we must also lengthen the scan sequence which decreases the temporal resolution. By comparing what can be reconstructed for with different scan sequences we can investigate this tradeoff and pick the most appropriate sequence.

Acknowledgements

We thank Angel Pineda for valuable discussions. This work was supported by NIH grants R01 CA52643 and P41 RR14304. A.L. was supported by NSF grant VIGRE 9977116.

References

1. M. Abramowitz and I. A. Stegun. *Handbook of Mathematical Functions with Formulas, Graphs, and Mathematical Tables*. US Government Printing Office, Washington, DC, 1964.
2. A. E. Albert. *Regression and the Moore-Penrose Pseudoinverse*. Academic Press, New York, 1972.
3. H. H. Barrett and K. J. Myers. *Foundations of Image Science*. Wiley, expected 2001.
4. M. Bertero and P. Boccacci. *Introduction to Inverse Problems in Imaging*. Institute of Physics Publishing, Bristol, 1998.
5. G. M. Boynton, S. A. Engel, G. H. Glover, and D. J. Heeger. Linear systems analysis of functional magnetic resonance imaging in human V1. *The Journal of Neuroscience*, 16(13):4207–4221, July 1996.

6. M. H. Buonocore, W. R. Brody, and A. Macovski. A natural pixel decomposition for two-dimensional image reconstruction. *IEEE Transactions on Biomedical Engineering*, 28(2):69–78, Feb. 1981.
7. E. Clarkson and H. Barrett. Bounds on null functions of linear digital imaging systems. *Journal of the Optical Society of America A – Optics, Image-Science and Vision*, 15(5):1355–1360, May 1998.
8. T. Q. Duong, D.-S. Kim, K. Uğurbil, and S.-G. Kim. Spatiotemporal dynamics of the BOLD fMRI signals: Toward mapping submillimeter cortical columns using the early negative response. *Magnetic Resonance in Medicine*, 44(2):231–242, Aug. 2000.
9. K. M. Hanson and G. W. Wecksung. Local basis-function approach to computed tomography. *Applied Optics*, 24(23):4028–39, Dec. 1985.
10. O. Josephs and R. N. A. Henson. Event-related functional magnetic resonance imaging: modelling, inference and optimization. *Philosophical Transactions of the Royal Society of London Series B – Biological Sciences*, 354(1387):1215–1228, July 1999.
11. R. M. Lewitt. Multidimensional digital image representations using generalized Kaiser-Bessel window functions. *Journal of the Optical Society of America A – Optics, Image-Science and Vision*, 7(10):1834–1846, Oct. 1990.
12. Z.-P. Liang and P. C. Lauterbur. *Principles of Magnetic Resonance Imaging: A Signal Processing Perspective*. IEEE Press, New York, 1999.
13. D. G. Nishimura. *Principles of Magnetic Resonance Imaging*. Published by the author, 1996.
14. L. Shepp and C.-H. Zhang. Fast functional magnetic resonance imaging via prolate wavelets. *Applied and Computational Harmonic Analysis*, 9(2):99–119, Sept. 2000.
15. A. W. Toga and J. C. Mazziotta, editors. *Brain Mapping: The Methods*. Academic Press, San Diego, 1996.
16. R. Van de Walle, H. H. Barrett, K. J. Myers, M. I. Altbach, B. Desplanques, A. F. Gmitro, J. Cornelis, and I. Lemahieu. Reconstruction of MR images from data acquired on a general non-regular grid by pseudoinverse calculation. *IEEE Transactions on Medical Imaging*, 19(12):1160–1167, Dec. 2000.
17. D. W. Wilson and H. H. Barrett. Decomposition of images and objects into measurement and null components. *Optics Express*, 2(6):254–260, Mar. 1998.